iScience

CellPress
OPEN ACCESS

Article

Identification of lysine-lactylated substrates in gastric cancer cells

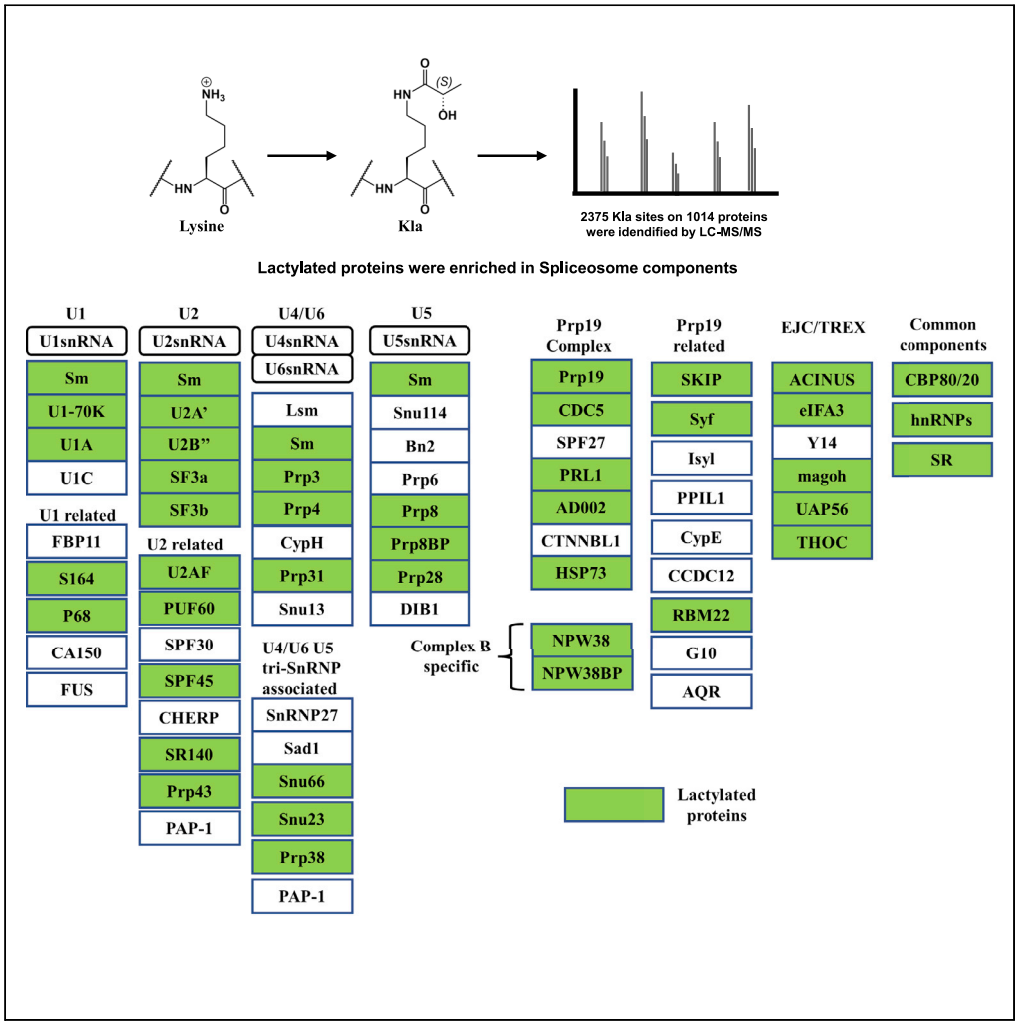

Dawei Yang, Jie Yin, Liuqun Shan, Xingling Yi, Wei Zhang, Yongbin Ding

weizhang@njmu.edu.cn (W.Z.)
njdyb@njmu.edu.cn (Y.D.)

Highlights

2375 Kla sites in 1014 proteins were identified in gastric cancer AGS cells

Lysine lactylation could be a prognostic marker in gastric cancer

Lactylated proteins were significantly enriched in spliceosome

Lactate could influence RNA splicing in gastric cancer AGS cells

Yang et al., iScience 25, 104630
July 15, 2022
https://doi.org/10.1016/j.isci.2022.104630

iScience

CellPress
OPEN ACCESS

Article

Identification of lysine-lactylated substrates in gastric cancer cells

Dawei Yang,[1,7] Jie Yin,[4,7] Liuqun Shan,[5] Xingling Yi,[6] Wei Zhang,[3,*] and Yongbin Ding[2,5,8,*]

SUMMARY

Cancer cells tend to utilize aerobic glycolysis to generate energy and metabolites; the end product of aerobic glycolysis is lactate, which promotes lysine lactylation (Kla). Kla is a newly discovered histone post-translational modification (PTM) that plays important roles in regulating gene expression. However, Kla in non-histone mammalian proteins is unclear. Here, a comprehensive analysis of lactylated proteins in gastric cancer AGS cells was conducted. There were 2375 Kla sites found in 1014 proteins. Interestingly, KEGG pathway analysis showed that these proteins were significantly enriched in spliceosome function. In addition, Kla was more abundant in gastric tumors than in adjacent tissues, and high levels of Kla in gastric tumors were associated with poor prognosis. These results suggest that Kla could be a prognostic marker in gastric cancer. This lysine lactylome analysis in gastric cancer cells, the first of its kind, provides a valuable foundation for further studies of Kla.

INTRODUCTION

Despite progress in available treatments, gastric carcinoma remains the third most common cause of cancer-related death worldwide (Joshi and Badgwell, 2021; Sung et al., 2021). Deeper understanding of the biological nature of this disease is therefore needed. The Warburg effect is one of the most common characteristics of cancers, including gastric carcinoma (Liu et al., 2019); this effect involves enhanced glycolysis and metabolism of pyruvate to lactate rather than oxidative phosphorylation under aerobic conditions. Lactate dehydrogenase A (LDHA), the key enzyme in lactogenesis, is a predictor of poor prognosis in patients with gastric cancer (Kolev et al., 2008). In addition, levels of lactate in gastric juice are correlated with tumor size and the degree of invasion in gastric cancer (Armstrong et al., 1984). Although lactate was recognized as a metabolic byproduct or energy source in previous studies, its non-metabolic functions in gastric cancer remain unclear.

In 2019, Zhao et al. reported lactate-derived histone lysine lactylation (Kla) as a novel post-translational modification (PTM) that stimulated gene transcription in macrophages (Zhang et al., 2019a). The functions of histone Kla were then explored in mouse embryo fibroblasts (MEFs) (Li et al., 2020a), ocular melanoma cells (Yu et al., 2021), and non-small cell lung cancer (NSCLC) cells (Jiang et al., 2021); these studies indicated that Kla has important effects in regulating pluripotency and oncogenesis. Few studies have focused on Kla of non-histone proteins, although such studies have been conducted in *Botrytis cinerea* and *Oryza sativa* (Gao et al., 2020; Meng et al., 2021). Yang et al. reported lactylation of HMGB1 in macrophages, but the specific lactylation sites were not studied (Yang et al., 2021). Thus, identification of lactylated substrates and specific lactylation sites in mammals should be conducted to help comprehend the non-metabolic functions of lactate.

Although basal lactate production averages ~0.8 mmol/kg body weight/h, the concentration can reach 12.9 mmol/kg body weight/h in glycolytic tumors (Vinasco et al., 2019; Walenta et al., 1997, 2000). Concentrations of lactate in gastric juice were shown to be higher in patients with gastric carcinoma than in those from control groups (Armstrong et al., 1984), suggesting that the concentration of lactate is higher in gastric tumors than in normal gastric tissues. In this study, we compared Kla abundance in gastric cancer and para-cancerous tissues from 76 patients by immunohistochemical staining (IHC). Levels of Kla were higher in human gastric tumors than that in adjacent gastric tissues and high levels of Kla in gastric tumors indicated poor prognosis in patients. We also performed proteomic analysis of gastric cancer cells and identified 2375 Kla sites in 1014 proteins, including a lactylation site in HMGB1. These lactylated proteins were distributed in multiple cellular compartments, with more than half localized to the nucleus. In

[1]Department of Pharmacy, The Second Hospital of Nanjing, Nanjing University of Chinese Medicine, Nanjing, Jiangsu 210003, China

[2]Department of General Surgery, Pukou Branch Hospital of Jiangsu Province Hospital (Nanjing Pukou Central Hospital), Nanjing, Jiangsu 211800, China

[3]Department of General Surgery, Jiangsu Province Hospital, The First Affiliated Hospital of Nanjing Medical University, Nanjing, Jiangsu 210029, China

[4]Department of General Surgery, Haian People's Hospital, Haian, Jiangsu 226600, China

[5]Department of General Surgery, The Second Hospital of Nanjing, Nanjing University of Chinese Medicine, Nanjing, Jiangsu 210003, China

[6]Micron Biotechnology Co., Ltd., Hangzhou 310051, China

[7]These authors contributed equally

[8]Lead contact

*Correspondence: weizhang@njmu.edu.cn (W.Z.), njdyb@njmu.edu.cn (Y.D.)

https://doi.org/10.1016/j.isci.2022.104630

addition, we identified 63 lactylated spliceosomal proteins, indicating that this PTM was abundant in the spliceosome and may affect RNA splicing.

Together, the results of this study validate the prognostic value of Kla in gastric cancer, expand the known profile of protein substrates and pathways affected by Kla, and provide a valuable foundation for further studies on functions of Kla in human diseases.

RESULTS

Systematic profiling of the Kla proteome in AGS cells

Although Kla can occur on non-histone proteins, proteome-wide identification of Kla substrates had not previously been conducted in mammalian cells. To identify proteins bearing Kla, we conducted a proteomic screen using affinity-directed mass spectrometry.

First, we confirmed Kla modifications in gastric cancer cells via Western blot. Lactate increased the abundance of Kla in AGS cells (Figure 1A). Multiple protein bands with different molecular weights were observed, indicating that many non-histone proteins were lactylated in gastric cancer cells (Figure 1A).

We then conducted affinity-directed mass spectrometry. Briefly, proteins were extracted from cells and digested with trypsin, and then the lactylated peptides were enriched with anti-Kla antibodies. Peptides were identified by liquid chromatography/tandem mass spectroscopy (LC-MS/MS) analysis and database searching (Figure 1B). To improve the reliability of identified sites, we filtered out peptides with MaxQuant scores below 40 and selected those with localization probabilities >0.75 as previously described (Huang et al., 2021). This led to the identification of 2375 high-confidence Kla sites in 1014 proteins (Table S1).

Among the 1014 proteins, about 52.7% contained single Kla sites, whereas 3.6% contained more than eight Kla sites, which corresponded to about 19.7% of all identified sites (Figure 1C). In addition, we identified 27 core histone Kla sites, including eight previously unknown sites (Table S2). We also identified the lactylated site in HMGB1; lactylation of this protein is associated with mortality due to sepsis (Yang et al., 2021). Representative MS/MS spectra of lactylated HMGB1 and H2AX are shown in Figure 1D. As shown in the upper panel in Figure 1D, 11 ions (y1 to y8 and b2 to b4) were detected, and ion b2 consisted of lysine and threonine. The mass to charge ratio (m/z) of b2 would be around 230.149 if the amino acids were not modified, but the actual m/z value of b2 was 302.17. This corresponds to a mass shift of 72.021, consistent with the shift caused by addition of a lactyl group (Zhang et al., 2019a). Ions b3 and b4 also had mass shifts of 72.021 while ions y1 to y8 did not. These results provided evidence that the first lysine of the KTSATVGPK sequence was lactylated.

Properties of Kla peptides in AGS cells

To define the possible Kla motifs in lactylated proteins, we compared the amino acid sequences surrounding confirmed Kla sites and identified 10 conserved motifs; xxxxxxxxxx_K_xxGxxxxxxx (present in 80 of the 1014 peptides), xxxKxxxxxx_K_xxxxxxxxxx (100 peptides), xxxxxxxxPx_K_xxxxxxxxxx (87 peptides), xxxxxxxxxx_K_xxxxxxxxKx (132 peptides), xxxxxxxxxx_K_xxxxxKxxx (152 peptides), xxxxxxxxxx_K_xxxxxRxxxx (149 peptides), xxxxxxxxxx_K_xxxxxKxxxx (202 peptides), xxxxxxxxxx_K_x-xxxKxxxxx (240 peptides), xxKxxxxxxx_K_xxxxxxxxxx (325 peptides), and xxxxxxxxxx_K_xxxxxxxKxx (274 peptides) (Figure 2A). These motifs differ from those identified in *O. sativa* and *B. cinerea* (Gao et al., 2020; Meng et al., 2021). Heatmaps of the amino acid sequences surrounding lactylation sites demonstrated that K residues were enriched in the regions from −10 to −3 and from 3 to 10, and that A residues were enriched in the regions from −8 to −1 and from 1 to 6 (Figure 2B).

Structure analysis was performed to investigate the correlation between Kla and protein structures in gastric cancer cells. Among the 2375 Kla sites, 2269 were located in regions with ordered secondary structures, 31% were located in alpha-helices, and 64% were located in coils (Figure 2C). In addition, lactylated sites in the protein surface were more likely to be exposed than other lysine residues (Figure 2D).

Characterization of the Kla proteome in AGS cells

To better characterize lactylated proteins in gastric cancer cells, we analyzed the subcellular localization of the lactylated substrates. More than half of the proteins (56.6%) were localized to the nucleus, whereas

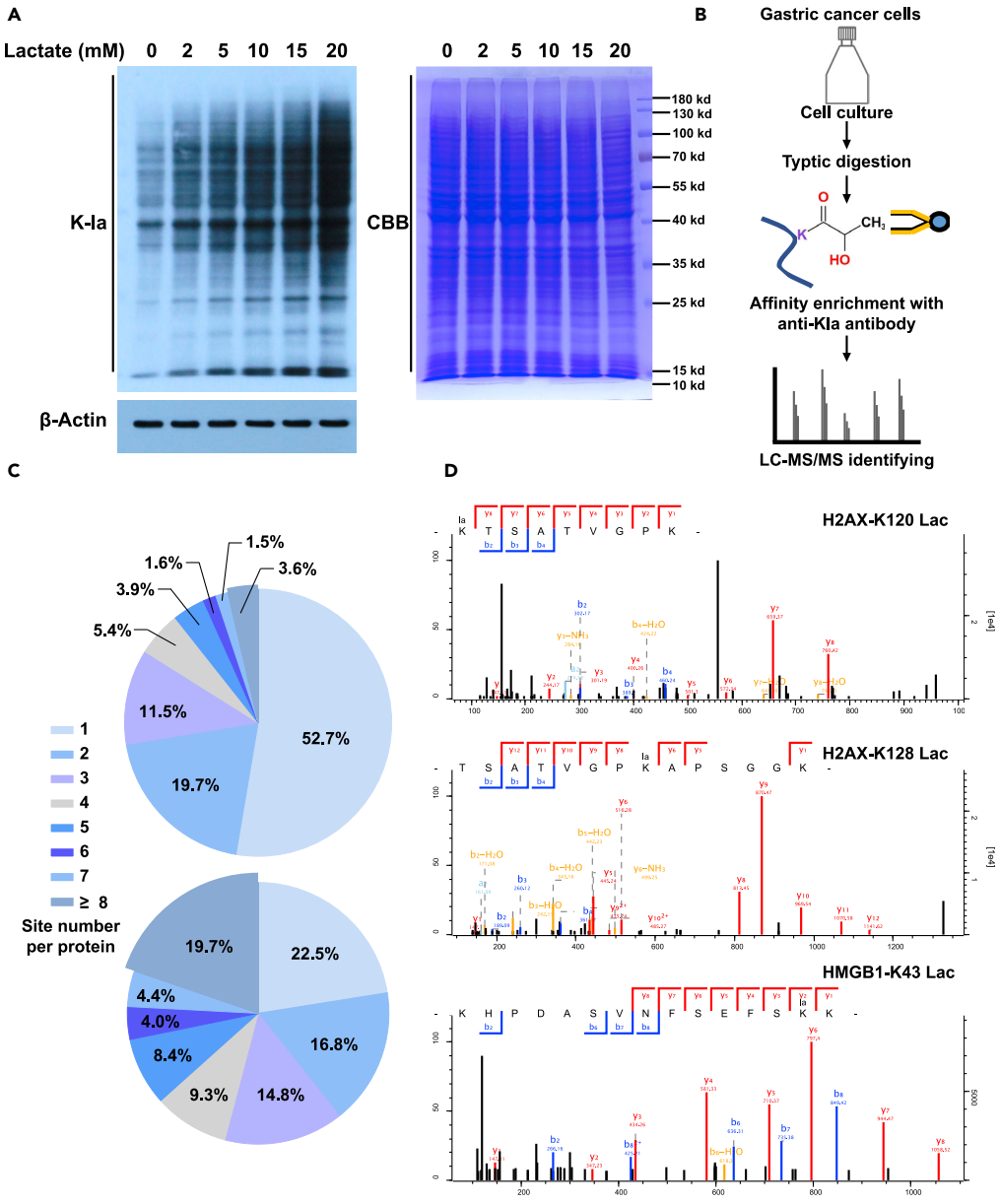

Figure 1. Systematic profiling of the Kla proteome

(A) Lactate increased lactylated proteins in gastric cancer AGS cells.

(B) A schematic flow chart for identification of Kla-containing protein substrates in AGS cells.

(C) Distribution of Kla proteins (above) and Kla sites (below) based on the number of sites per protein.

(D) Tandem mass spectroscopy (MS/MS) spectra of three representative Kla peptides from HMGB1 and H2AX.

29.3% and 5.2% were distributed in the cytoplasm and mitochondria, respectively (Figure 3A). We then conducted biochemical pathway analysis using annotations from the Kyoto Encyclopedia of Genes and Genomes (KEGG). This analysis showed that proteins related to the spliceosome were more likely to be lactylated (Figure 3B), suggesting that Kla may affect RNA splicing. This finding was further supported by analysis of Gene Ontology (GO) functional annotations; analysis of the biological processes associated with lactylated proteins showed enrichment proteins that participate in RNA processing or splicing (Figure 3C); enrichment analysis of molecular functions also showed that proteins involved in RNA binding were more likely to be lactylated (Figure 3D). Meanwhile, immunoprecipitation was used to confirm

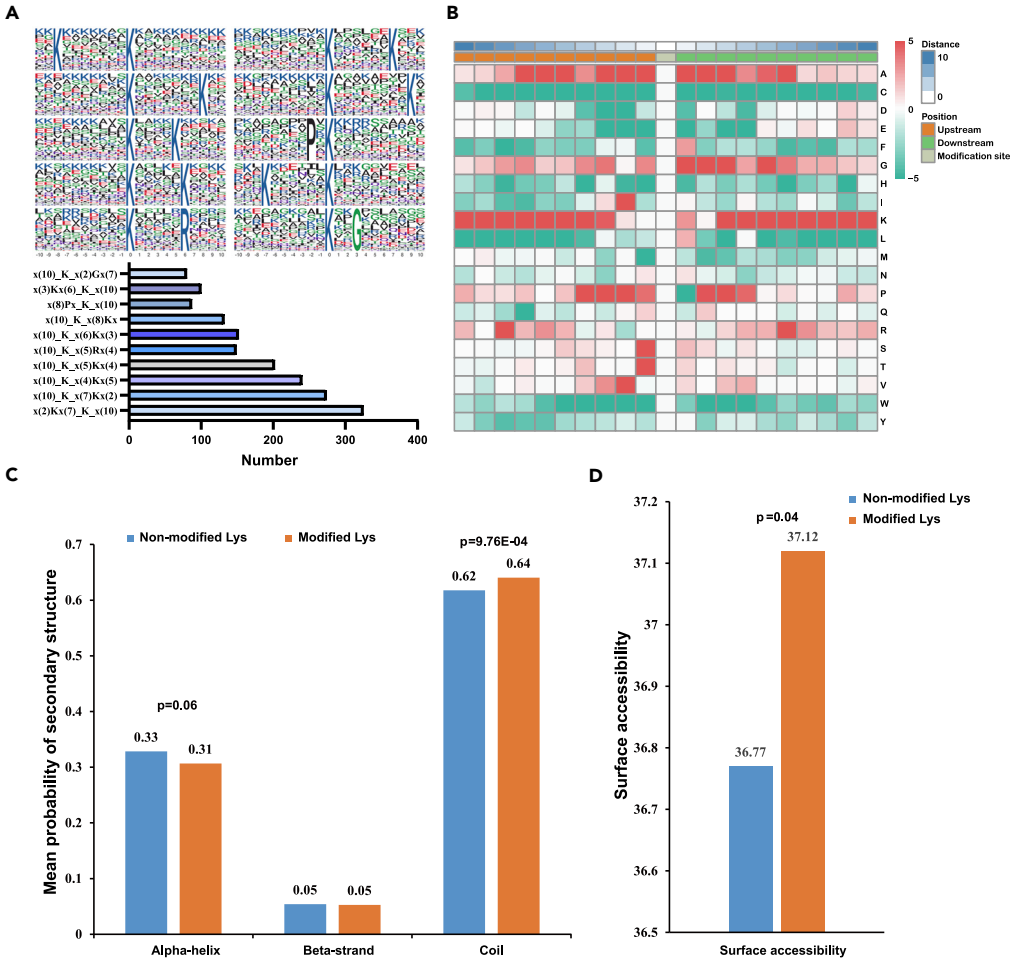

Figure 2. Properties of Kla peptides

(A) Sequence motif logo showing a representative sequence for all Kla sites. The central K represents the lactylated lysine. The number of instances of each conserved motif in the samples from the present study is shown below.

(B) Heatmap of the amino acid composition around Kla sites. Green indicates low frequency of an amino acid and red indicates high frequency.

(C) Estimated probabilities of Kla sites in of coil, beta-strand, and alpha-helix structures.

(D) Estimated surface accessibility of Kla sites in substrates. p values were calculated with Fisher's exact test.

lactylation of hnRNPA1 and SF3B1 (Figure S1), which are key proteins that regulate alternative splicing (Howard et al., 2018; Liu et al., 2020).

The results support that Kla is abundant in spliceosomal proteins in these gastric cancer cells. A summary of lactylated proteins related to the spliceosome is shown in Figure 3E.

Lactate changed RNA splicing events in AGS cells

Because Kla proteins were enriched in spliceosome functions, we predicted that lactate may affect RNA splicing in gastric cancer cells. We therefore performed an RNA-seq analysis using the program rMATS (Hwang et al., 2020). The presence of lactate altered RNA splicing events (Figure 4A), including skipped exon (SE), alternative 5′ splice site (A5SS), alternative 3′ splice site (A3SS), mutually exclusive exons (MXE), and retained intron (RI) events in AGS cells (Table S3). RNA splicing events are visualized as volcano plots in Figures 4B–4F.

Pan-kla was more abundant in gastric tumors than that in adjacent tissues

Kla substrates were identified in our proteomic screening of gastric tumor cells. However, whether this type of PTM is correlated with gastric tumors has not yet been determined. We therefore examined Kla levels by

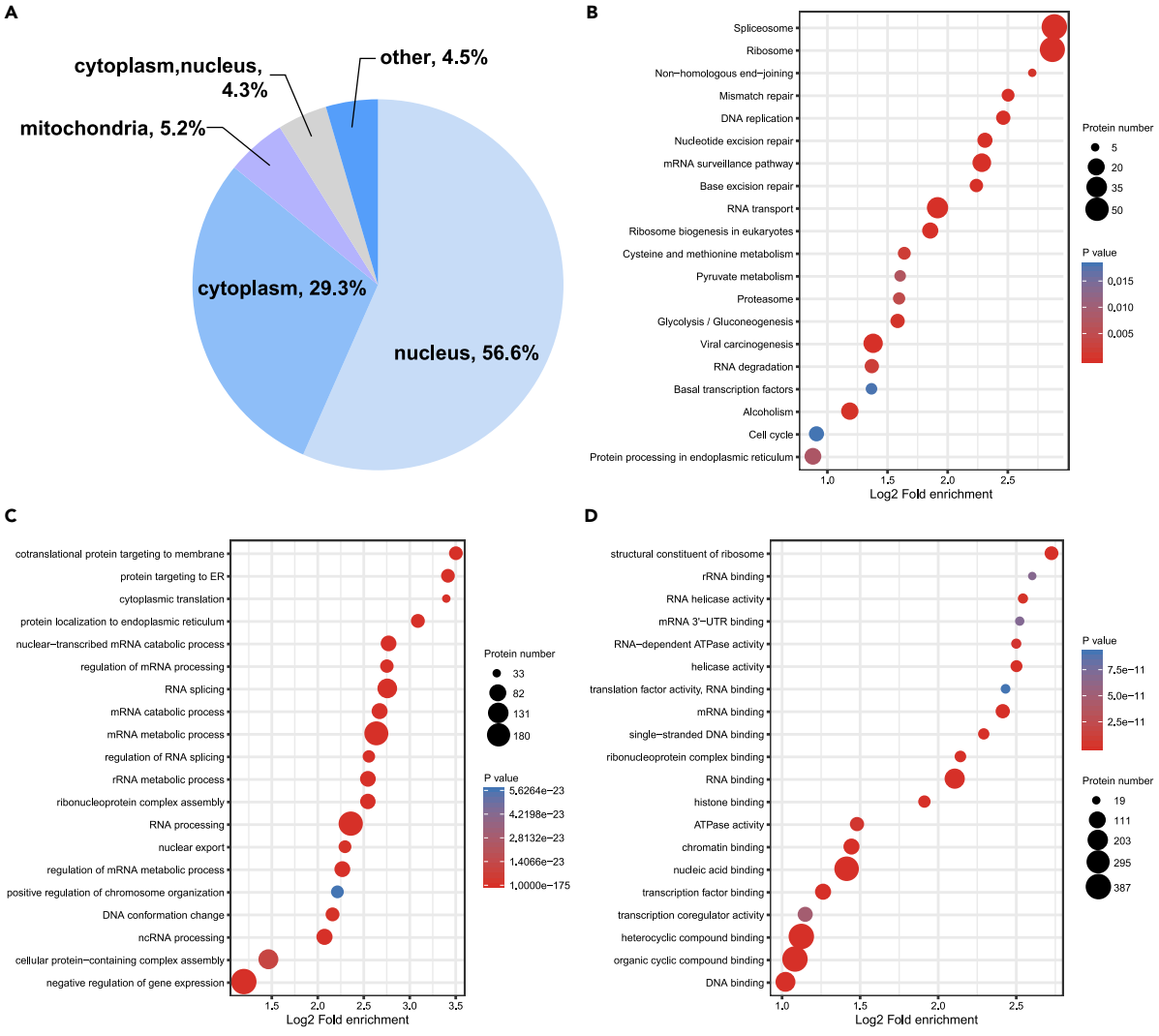
A
cytoplasm,nucleus, 4.3%
other, 4.5%
mitochondria, 5.2%
cytoplasm, 29.3%
nucleus, 56.6%
B
Spliceosome
Ribosome
Non−homologous end−joining
Mismatch repair
DNA replication
Nucleotide excision repair
mRNA surveillance pathway
Base excision repair
RNA transport
Ribosome biogenesis in eukaryotes
Cysteine and methionine metabolism
Pyruvate metabolism
Proteasome
Glycolysis / Gluconeogenesis
Viral carcinogenesis
RNA degradation
Basal transcription factors
Alcoholism
Cell cycle
Protein processing in endoplasmic reticulum
1.0
1.5
2.0
2.5
Log2 Fold enrichment
Protein number
5
20
35
50
P value
0.015
0.010
0.005
C
cotranslational protein targeting to membrane
protein targeting to ER
cytoplasmic translation
protein localization to endoplasmic reticulum
nuclear−transcribed mRNA catabolic process
regulation of mRNA processing
RNA splicing
mRNA catabolic process
mRNA metabolic process
regulation of RNA splicing
rRNA metabolic process
ribonucleoprotein complex assembly
RNA processing
nuclear export
regulation of mRNA metabolic process
positive regulation of chromosome organization
DNA conformation change
ncRNA processing
cellular protein−containing complex assembly
negative regulation of gene expression
1.5
2.0
2.5
3.0
3.5
Log2 Fold enrichment
Protein number
33
82
131
180
P value
5.6264e−23
4.2198e−23
2.8132e−23
1.4066e−23
1.0000e−175
D
structural constituent of ribosome
rRNA binding
RNA helicase activity
mRNA 3'−UTR binding
RNA−dependent ATPase activity
helicase activity
translation factor activity, RNA binding
mRNA binding
single−stranded DNA binding
ribonucleoprotein complex binding
RNA binding
histone binding
ATPase activity
chromatin binding
nucleic acid binding
transcription factor binding
transcription coregulator activity
heterocyclic compound binding
organic cyclic compound binding
DNA binding
1.0
1.5
2.0
2.5
Log2 Fold enrichment
P value
7.5e−11
5.0e−11
2.5e−11
Protein number
19
111
203
295
387
E
SPLICEOSOME
5' splice site
Branch point
3' splice site
pre-mRNA
Exon
GU
A
AG
Exon
Intron
Common components
mRNA
Post-spliceosomal complex
complex A
complex B
complex C
Activated spliceosome complex B*
U4/U6.U5 tri-snRNP
FRP19 complex
EJC/TREX
1st step
2nd step
Spliceosome components
U1
U2
U4/U6
U5
Prp19 complex
Prp19 related
EJC/TREX
Common components
Complex B specific
U4/U6 snRNP
U6 snRNA
U4 snRNA
Sm
Lsm

Figure 3. Characteristics of the Kla proteome in AGS cells

(A) The subcellular distribution of Kla proteins.

(B) Kyoto Encyclopedia of Genes and Genomes (KEGG) pathway enrichment analysis of Kla proteins.

(C and D) Gene Ontology (GO) enrichment analysis of Kla proteins according to (C) biological processes and (D) molecular functions.

(E) Wiring diagrams showing the Kla proteins enriched in the spliceosomal pathway (https://www.kegg.jp/kegg/pathway.html).

IHC in a tissue microarray, which included 76 gastric tumor sections and corresponding para-cancerous sections. The results showed that among the 76 samples, Kla levels were significantly higher in 51 tumor tissues than their corresponding para-cancerous tissues (Figures 5A and 5B). Furthermore, three gastric cancer cell lines showed higher Kla levels and sensitivity to lactate dehydrogenase (LDH) inhibition than gastric epithelial cells (Figure S2). We also studied the relationships between Kla levels in tumor tissues and patient age/level of tumor differentiation. Kla was more abundant in poorly differentiated tumors than in the moderately differentiated tumors (Figure 5C). Pearson correlation analysis suggested that age was not correlated with Kla abundance (Figure 5D, $p = 0.2874$).

Pan-Kla abundance predicted prognosis in gastric tumor patients

The above results showed that Kla was more abundant in tumor tissues than in adjacent tissues, we therefore then examined whether Kla levels were correlated with patient prognosis. Using TNM staging, those with Stage IIIA-IIIB (TNM staging) gastric carcinoma had higher Kla levels than those with Stage I-II carcinoma (Figure 5E). Tumors from patients with lymph node metastasis were also more lactylated than those from patients without lymph node metastasis (Figure 5F). Kaplan-Meier analysis was conducted, which confirmed that high Kla levels were correlated with poor overall survival in patients with gastric cancer (Figure 5G). The hazard ratios of Kla levels and differentiated levels against overall survival were 2.77 and 0.56, respectively, in a multivariate Cox regression proportional hazards model (Figure 5H).

DISCUSSION

As the primary byproduct of the Warburg effect, lactate has long been associated with tumors. The tumor-promoting actions of lactate include regulating immune surveillance (Brand et al., 2016; Colegio et al., 2014; Peng et al., 2016; Zhang et al., 2019b), accelerating tumor angiogenesis (Giatromanolaki et al., 2006; Kolev et al., 2008; Shi et al., 2001; Vegran et al., 2011), promoting metastasis (Cantelmo et al., 2016; Tasdogan et al., 2020), and even affecting fibroblasts (Formby and Stern, 2003; Stern et al., 2002). The effects of lactate on PTM that may mediate these processes were not discovered until 2019 (Zhang et al., 2019a). Lactate was found in 2014 to promote the transcription of *Arg1* and *Vegfa* in macrophages (Colegio et al., 2014), but the mechanism remained unclear. In 2019, Zhao et al. found that histone lactylation controlled the transcription of *Arg1* and *Vegfa* (Zhang et al., 2019a), and further elucidated the effects of lactate on macrophage polarization. Kla was also found to occur in non-histone proteins. Gao et al. identified 273 kla sites in 166 proteins in *B. cinerea* (Gao et al., 2020), and Meng et al. identified 638 kla sites in 342 proteins in rice grains, suggesting that Kla could be associated with fugal pathogenicity and carbon metabolism. Moreover, Yang et al. reported lactylation of HMGB1 in macrophages, but the specific lactylation sites in HMGB1 were not studied (Yang et al., 2021). Thus, Kla substrate sites in non-histone proteins have remained unknown in the context of human diseases. In this study, we identified 2375 Kla sites in 1014 proteins in AGS cells, including eight previously unknown histone Kla sites and a lactylated site in HMGB1.

The maturation of precursor mRNA (pre-mRNA) relies on RNA splicing, which removes introns and exons from pre-mRNA (Kitamura and Nimura, 2021). Alternative splicing increases the diversity of proteins by affecting the complexity of mRNA, and is known to regulate multiple cellular progress (Zhang et al., 2021). It was previously reported that RNA splicing could affect lactate metabolism (Klipfel et al., 2021; Leyva-Carrillo et al., 2019; Li et al., 2020b); however, whether lactate could affect RNA splicing was unknown. We have identified 193 Kla sites in 70 spliceosome-related proteins. KEGG pathway analysis showed that lactylated proteins were enriched in spliceosome functions, suggesting a global influence of lactate on RNA splicing. Moreover, as shown in the RNA-seq analysis, treatment with lactate caused differential splicing events (namely SE, A5SS, A3SS, MXE, and RI) to occur in AGS cells.

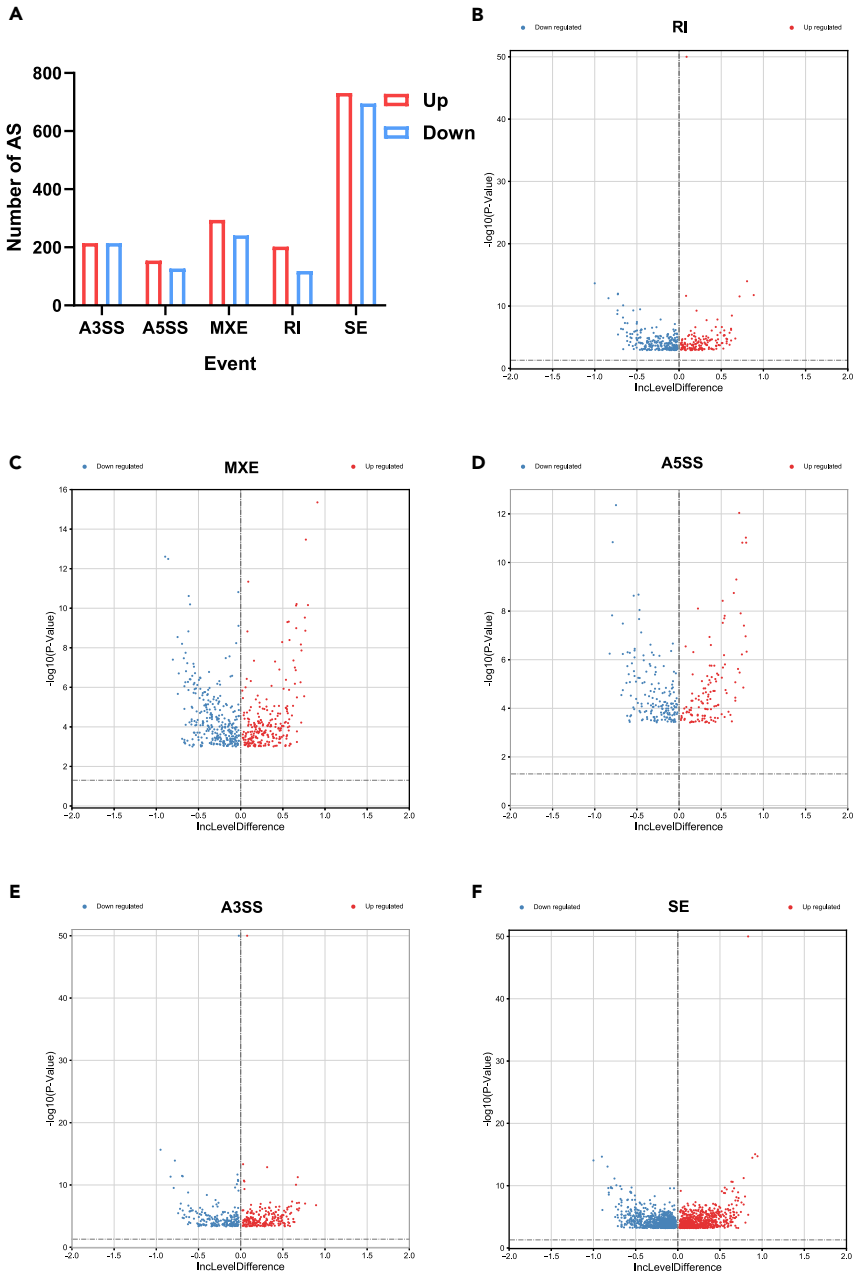

Figure 4. Lactate treatment caused differential alternate splicing (AS) events in AGS cells

AGS cells were treated with 20 mM lactate or vehicle for 24 h.

(A) Numbers of AS events altered by lactate treatment.

(B–F) Volcano plots show how lactate treatment altered different types of AS events, namely (B) Retained intron (RI), (C) Mutually exclusive exon (MXE), (D) Alternative 5′ splice site (A5SS), (E) Alternative 3′ splice site (A3SS), and (F) Skipped exon (SE) events.

Finally, we compared pan-Kla levels in gastric tumors and adjacent tissues. Kla levels were significantly higher in 51 tumor tissues than in the corresponding para-cancerous tissues. In addition, higher levels of Kla were correlated with more poorly differentiated tumors, lymph node metastasis, and poorer overall patient survival rates. In summary, this study not only suggests a prognostic value of Kla in gastric tumors but also identified Kla substrates via LC-MS/MS. As the first lysine lactylome analysis in mammalian cells, our findings provide a valuable foundation for further studies related to the function of Kla in human diseases.

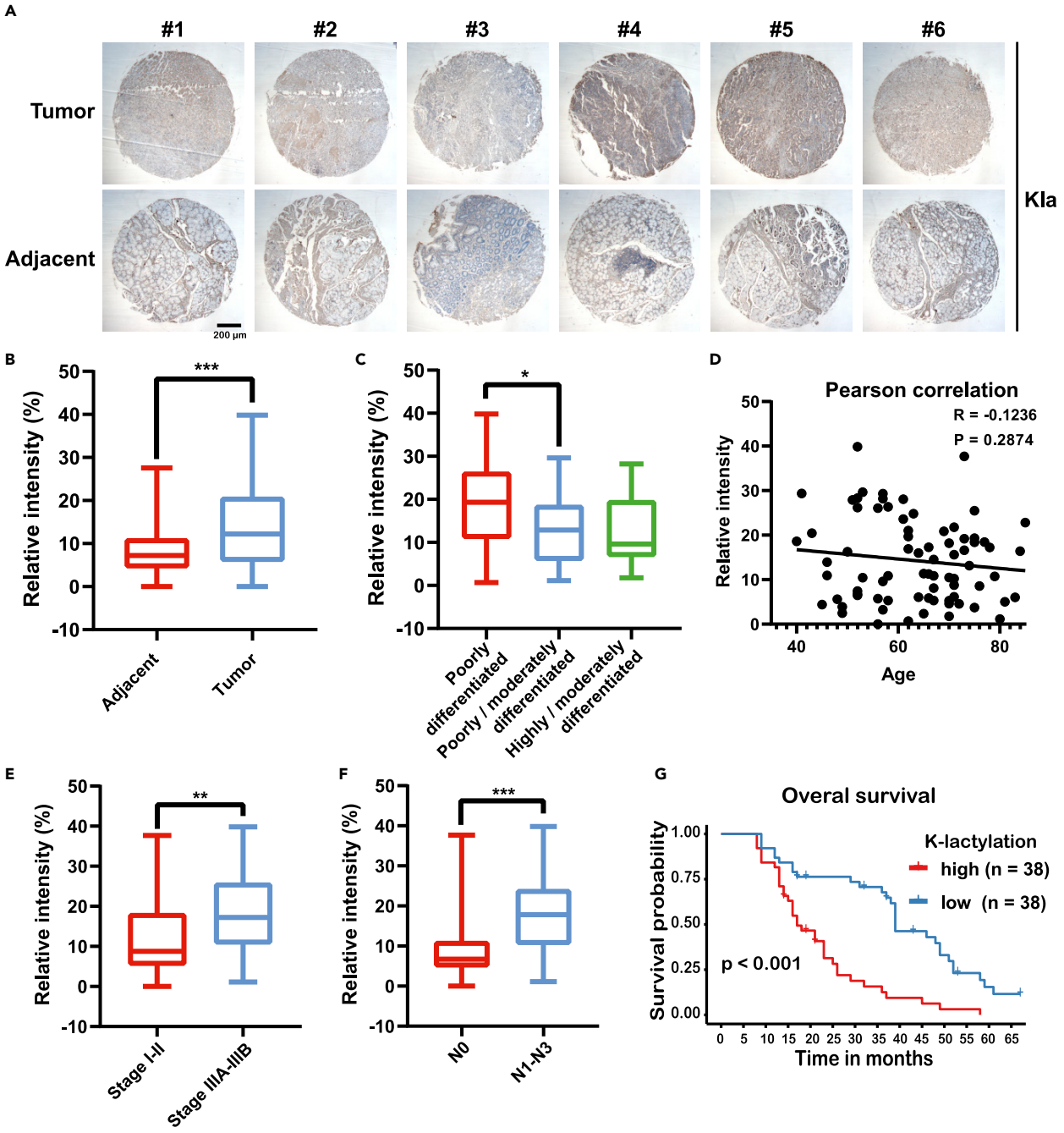

H

Prognostic factor	HR	*P* value	95% CI
Lysine-Lactylation (High)	2.77	0.001	1.47 to 5.26
Genders (Male)	1.73	0.091	0.92 to 3.26
Age	0.98	0.128	0.95 to 1.01
Differentiated Level	0.56	0.004	0.38 to 0.83

Figure 5. Kla abundance in gastric tumors and its relationship with the prognosis

(A and B) Representative images and quantification of immunohistochemistry (IHC) staining of Kla in gastric tumors (n = 76) or adjacent tissues (n = 76). Relative intensities of IHC staining were determined with Image Pro Plus v6.0.

(C) Relative Kla levels in types of gastric tumors: poorly differentiated (n = 27), moderately/poorly differentiated (n = 26), and moderately/highly differentiated (n = 11).

(D) Relative Kla levels in gastric tumors from patients of varying ages (n = 76).

(E) Relative Kla levels in gastric tumors from patients with TNM stages I-II (n = 39) and stages IIIA-IIIB (n = 37).

(F) Relative Kla levels in gastric tumors from patients with lymphatic metastasis (N1, N2, and N3; n = 46) or without lymphatic metastasis (N0; n = 29).

(G) Survival rates for patients with different Kla levels using Kaplan-Meier analysis.

(H) A multivariate Cox regression proportional hazards model was used to analyze the hazard factors in gastric cancer. Students' T test was employed in Figures 1B and 1D–1F to compare the differences between groups; One-way ANOVA was used in Figure 1C to compare the differences between groups; Significance values are *p < 0.05, **p < 0.01 and ***p < 0.001.

Limitations of the study

The underlying mechanism of how Kla affects gastric cancer progression was not investigated here. Future studies, which should include genetic manipulation and mutagenesis experiments, are needed to verify the effects of Kla on protein functions and tumor progression.

DATA AVAILABILITY

All data generated or analyzed during this study are included in this article.

ETHICS STATEMENT

Tissue arrays were provided by the Nanjing Pukou Central Hospital and approved by Ethics Committee of the Nanjing Pukou Central Hospital.

STAR★METHODS

Detailed methods are provided in the online version of this paper and include the following:

- KEY RESOURCES TABLE
- RESOURCE AVAILABILITY
  - Lead contact
  - Materials availability
  - Data and code availability
- EXPERIMENTAL MODEL AND SUBJECT DETAILS
  - Cell lines
- METHOD DETAILS
  - Western blot
  - RNA-seq
  - Immunoprecipitation (IP)
  - Immunohistochemistry (IHC) staining
  - Sample preparation for LC-MS/MS
  - Peptide fractionation and affinity enrichment
  - LC-MS/MS analysis
  - Database searching
  - Bioinformatics analysis
- QUANTIFICATION AND STATISTICAL ANALYSIS

SUPPLEMENTAL INFORMATION

Supplemental information can be found online at https://doi.org/10.1016/j.isci.2022.104630.

ACKNOWLEDGMENTS

We thank Dr. Lei Li and Peng Wang for the help in the immunohistochemistry. This research was supported by the Program of clinical medicine expert team of Suzhou (grant number SZYJTD201824), Social Development Project of Jiangsu Provincial Science and Technology Department (BE2018698), and Medical engineering cooperation project of Nanjing Municipal Science and Technology Bureau (202110032).

AUTHOR CONTRIBUTIONS

Dawei Yang: Conceptualization, Methodology, Investigation, Writing – original draft. Jie Yin: Methodology, Software. Liuqun Shan: Writing – review & editing. Xingling Yi: Methodology. Wei Zhang: Methodology, Writing – review & editing, Funding acquisition. Yongbin ding: Conceptualization, Writing – review & editing, Resources, Supervision, Funding acquisition.

DECLARATION OF INTERESTS

The authors declare that they have no conflict of interest. Each listed author on the manuscript is aware of and agrees to the contents of the manuscript, including the authorship.

Received: January 31, 2022
Revised: May 26, 2022
Accepted: June 13, 2022
Published: July 15, 2022

REFERENCES

Armstrong, C.P., Dent, D.M., Berman, P., and Aitken, R.J. (1984). The relationship between gastric carcinoma and gastric juice lactate (L + D) and lactate dehydrogenase. Am. J. Gastroenterol. *79*, 675–678.

Brand, A., Singer, K., Koehl, G.E., Kolitzus, M., Schoenhammer, G., Thiel, A., Matos, C., Bruss, C., Klobuch, S., Peter, K., et al. (2016). LDHA-associated lactic acid production blunts tumor immunosurveillance by T and NK cells. Cell Metabol. *24*, 657–671. https://doi.org/10.1016/j.cmet.2016.08.011.

Cantelmo, A.R., Conradi, L.C., Brajic, A., Goveia, J., Kalucka, J., Pircher, A., Chaturvedi, P., Hol, J., Thienpont, B., Teuwen, L.A., et al. (2016). Inhibition of the glycolytic activator PFKFB3 in endothelium induces tumor vessel normalization, impairs metastasis, and improves chemotherapy. Cancer Cell *30*, 968–985. https://doi.org/10.1016/j.ccell.2016.10.006.

Colegio, O.R., Chu, N.Q., Szabo, A.L., Chu, T., Rhebergen, A.M., Jairam, V., Cyrus, N., Brokowski, C.E., Eisenbarth, S.C., Phillips, G.M., et al. (2014). Functional polarization of tumour-associated macrophages by tumour-derived lactic acid. Nature *513*, 559–563. https://doi.org/10.1038/nature13490.

Formby, B., and Stern, R. (2003). Lactate-sensitive response elements in genes involved in hyaluronan catabolism. Biochem. Biophys. Res. Commun. *305*, 203–208. https://doi.org/10.1016/s0006-291x(03)00723-x.

Gao, M., Zhang, N., and Liang, W. (2020). Systematic analysis of lysine lactylation in the plant fungal pathogen Botrytis cinerea. Front. Microbiol. *11*, 594743. https://doi.org/10.3389/fmicb.2020.594743.

Giatromanolaki, A., Sivridis, E., Gatter, K.C., Turley, H., Harris, A.L., and Koukourakis, M.I.; Tumour, and Angiogenesis Research, G (2006). Lactate dehydrogenase 5 (LDH-5) expression in endometrial cancer relates to the activated VEGF/VEGFR2(KDR) pathway and prognosis. Gynecol. Oncol. *103*, 912–918. https://doi.org/10.1016/j.ygyno.2006.05.043.

Howard, J.M., Lin, H., Wallace, A.J., Kim, G., Draper, J.M., Haeussler, M., Katzman, S., Toloue, M., Liu, Y., and Sanford, J.R. (2018). HNRNPA1 promotes recognition of splice site decoys by U2AF2 in vivo. Genome Res. *28*, 689–698. https://doi.org/10.1101/gr.229062.117.

Huang, H., Zhang, D., Weng, Y., Delaney, K., Tang, Z., Yan, C., Qi, S., Peng, C., Cole, P.A., Roeder, R.G., and Zhao, Y. (2021). The regulatory enzymes and protein substrates for the lysine beta-hydroxybutyrylation pathway. Sci. Adv. *7*, eabe2771. https://doi.org/10.1126/sciadv.abe2771.

Hwang, J.Y., Jung, S., Kook, T.L., Rouchka, E.C., Bok, J., and Park, J.W. (2020). rMAPS2: an update of the RNA map analysis and plotting server for alternative splicing regulation. Nucleic Acids Res. *48*, W300–W306. https://doi.org/10.1093/nar/gkaa237.

Jiang, J., Huang, D., Jiang, Y., Hou, J., Tian, M., Li, J., Sun, L., Zhang, Y., Zhang, T., Li, Z., et al. (2021). Lactate modulates cellular metabolism through histone lactylation-mediated gene expression in non-small cell lung cancer. Front. Oncol. *11*, 647559. https://doi.org/10.3389/fonc.2021.647559.

Joshi, S.S., and Badgwell, B.D. (2021). Current treatment and recent progress in gastric cancer. CA A Cancer J. Clin. *71*, 264–279. https://doi.org/10.3322/caac.21657.

Kitamura, K., and Nimura, K. (2021). Regulation of RNA splicing: aberrant splicing regulation and therapeutic targets in cancer. Cells *10*, 923. https://doi.org/10.3390/cells10040923.

Klipfel, L., Cordonnier, M., Thiebault, L., Clerin, E., Blond, F., Millet-Puel, G., Mohand-Said, S., Goureau, O., Sahel, J.A., Nandrot, E.F., and Leveillard, T. (2021). A splice variant in SLC16A8 gene leads to lactate transport deficit in human iPS cell-derived retinal pigment epithelial cells. Cells *10*, 179. https://doi.org/10.3390/cells10010179.

Kolev, Y., Uetake, H., Takagi, Y., and Sugihara, K. (2008). Lactate dehydrogenase-5 (LDH-5) expression in human gastric cancer: association with hypoxia-inducible factor (HIF-1α) pathway, angiogenic factors production and poor prognosis. Ann. Surg Oncol. *15*, 2336–2344. https://doi.org/10.1245/s10434-008-9955-5.

Leyva-Carrillo, L., Hernandez-Palomares, M., Valenzuela-Soto, E.M., Figueroa-Soto, C.G., and Yepiz-Plascencia, G. (2019). Purification and partial biochemical characterization of recombinant lactate dehydrogenase 1 (LDH-1) of the white shrimp Litopenaeus vannamei. Protein Expr. Purif. *164*, 105461. https://doi.org/10.1016/j.pep.2019.105461.

Li, L., Chen, K., Wang, T., Wu, Y., Xing, G., Chen, M., Hao, Z., Zhang, C., Zhang, J., Ma, B., et al. (2020a). Glis1 facilitates induction of pluripotency via an epigenome-metabolome-epigenome signalling cascade. Nat. Metab. *2*, 882–892. https://doi.org/10.1038/s42255-020-0267-9.

Li, N., Kang, Y., Wang, L., Huff, S., Tang, R., Hui, H., Agrawal, K., Gonzalez, G.M., Wang, Y., Patel, S.P., and Rana, T.M. (2020b). ALKBH5 regulates anti-PD-1 therapy response by modulating lactate and suppressive immune cell accumulation in tumor microenvironment. Proc. Natl. Acad. Sci. USA *117*, 20159–20170. https://doi.org/10.1073/pnas.1918986117.

Liu, Y., Zhang, Z., Wang, J., Chen, C., Tang, X., Zhu, J., and Liu, J. (2019). Metabolic reprogramming results in abnormal glycolysis in gastric cancer: a review. OncoTargets Ther. *12*, 1195–1204. https://doi.org/10.2147/OTT.S189687.

Liu, Z., Yoshimi, A., Wang, J., Cho, H., Chun-Wei Lee, S., Ki, M., Bitner, L., Chu, T., Shah, H., Liu, B., et al. (2020). Mutations in the RNA splicing factor SF3B1 promote tumorigenesis through MYC stabilization. Cancer Discov. *10*, 806–821. https://doi.org/10.1158/2159-8290.CD-19-1330.

Meng, X., Baine, J.M., Yan, T., and Wang, S. (2021). Comprehensive analysis of lysine lactylation in rice (Oryza sativa) grains. J. Agric. Food Chem. *69*, 8287–8297. https://doi.org/10.1021/acs.jafc.1c00760.

Peng, M., Yin, N., Chhangawala, S., Xu, K., Leslie, C.S., and Li, M.O. (2016). Aerobic glycolysis promotes T helper 1 cell differentiation through an epigenetic mechanism. Science *354*, 481–484. https://doi.org/10.1126/science.aaf6284.

Shi, Q., Le, X., Wang, B., Abbruzzese, J.L., Xiong, Q., He, Y., and Xie, K. (2001). Regulation of vascular endothelial growth factor expression by

acidosis in human cancer cells. Oncogene *20*, 3751–3756. https://doi.org/10.1038/sj.onc.1204500.

Stern, R., Shuster, S., Neudecker, B.A., and Formby, B. (2002). Lactate stimulates fibroblast expression of hyaluronan and CD44: the Warburg effect revisited. Exp. Cell Res. *276*, 24–31. https://doi.org/10.1006/excr.2002.5508.

Sung, H., Ferlay, J., Siegel, R.L., Laversanne, M., Soerjomataram, I., Jemal, A., and Bray, F. (2021). Global cancer statistics 2020: GLOBOCAN estimates of incidence and mortality worldwide for 36 cancers in 185 countries. CA A Cancer J. Clin. *71*, 209–249. https://doi.org/10.3322/caac.21660.

Tasdogan, A., Faubert, B., Ramesh, V., Ubellacker, J.M., Shen, B., Solmonson, A., Murphy, M.M., Gu, Z., Gu, W., Martin, M., et al. (2020). Metabolic heterogeneity confers differences in melanoma metastatic potential. Nature *577*, 115–120. https://doi.org/10.1038/s41586-019-1847-2.

Végran, F., Boidot, R., Michiels, C., Sonveaux, P., and Feron, O. (2011). Lactate influx through the endothelial cell monocarboxylate transporter MCT1 supports an NF-kappa B/IL-8 pathway that drives tumor angiogenesis. Cancer Res. *71*, 2550–2560. https://doi.org/10.1158/0008-5472.Can-10-2828.

Vinasco, K., Mitchell, H.M., Kaakoush, N.O., and Castaño-Rodríguez, N. (2019). Microbial carcinogenesis: lactic acid bacteria in gastric cancer. Biochim. Biophys. Acta Rev. Canc *1872*, 188309. https://doi.org/10.1016/j.bbcan.2019.07.004.

Walenta, S., Salameh, A., Lyng, H., Evensen, J.F., Mitze, M., Rofstad, E.K., Mueller-Klieser, W., and SAlAmeh, A. (1997). Correlation of high lactate levels in head and neck tumors with incidence of metastasis. Am. J. Pathol. *150*, 409–415.

Walenta, S., Wetterling, M., Lehrke, M., Schwickert, G., Sundfør, K., Rofstad, E.K., and Mueller-Klieser, W. (2000). High lactate levels predict likelihood of metastases, tumor recurrence, and restricted patient survival in human cervical cancers. Cancer Res. *60*, 916–921.

Yang, K., Fan, M., Wang, X., Xu, J., Wang, Y., Tu, F., Gill, P.S., Ha, T., Liu, L., Williams, D.L., and Li, C. (2021). Lactate promotes macrophage HMGB1 lactylation, acetylation, and exosomal release in polymicrobial sepsis. Cell Death Differ. *29*, 133–146. https://doi.org/10.1038/s41418-021-00841-9.

Yu, J., Chai, P., Xie, M., Ge, S., Ruan, J., Fan, X., and Jia, R. (2021). Histone lactylation drives oncogenesis by facilitating m(6)A reader protein YTHDF2 expression in ocular melanoma. Genome Biol. *22*, 85. https://doi.org/10.1186/s13059-021-02308-z.

Zhang, D., Tang, Z., Huang, H., Zhou, G., Cui, C., Weng, Y., Liu, W., Kim, S., Lee, S., Perez-Neut, M., et al. (2019a). Metabolic regulation of gene expression by histone lactylation. Nature *574*, 575–580. https://doi.org/10.1038/s41586-019-1678-1.

Zhang, W.N., Wang, G.H., Xu, Z.G., Tu, H.Q., Hu, F.Q., Dai, J., Chang, Y., Chen, Y.Q., Lu, Y.J., Zeng, H.L., et al. (2019b). Lactate is a natural suppressor of RLR signaling by targeting MAVS. Cell *178*, 176–189.e15. https://doi.org/10.1016/j.cell.2019.05.003.

Zhang, Y., Qian, J., Gu, C., and Yang, Y. (2021). Alternative splicing and cancer: a systematic review. Signal Transduct. Target. Ther. *6*, 78. https://doi.org/10.1038/s41392-021-00486-7.

STAR★METHODS

KEY RESOURCES TABLE

REAGENT or RESOURCE	SOURCE	IDENTIFIER
Antibodies		
Anti-Kla antibody	Micron Biotechnology Company	Cat# WM101; RRID: Not applicable
Anti-hnRNPA1 antibody	ABclonal	Cat# A11564; RRID:AB_2861599
Anti-SF3B1 antibody	ABclonal	Cat# A15801; RRID:AB_2763223
Anti-β-Actin	ABclonal	Cat# AC026; RRID:AB_2768234
HRP Goat Anti-Rabbit IgG secondary antibody	ABclonal	Cat# AS014; RRID:AB_2769854
Rabbit Control IgG	ABclonal	Cat# AC005; RRID:AB_2771930
Biological samples		
Tissue arrays	Nanjing Pukou Central Hospital	Not applicable
Chemicals, peptides, and recombinant proteins		
Sodium lactate	Aladdin Biochemical Technology	Cat# S108838
ECL substrate	Yeasen	Cat# 36222ES60
Urea	Sigma	Cat# U5378
NP40	Sigma	Cat# I3021
Sodium deoxycholate	Sigma	Cat# 30970
EDTA	Sigma	Cat# E6758
Dithiothreitol	Solarbio	Cat# D8220
Glycine	Solarbio	Cat# G8200
Tris	Solarbio	Cat# T8060
SDS	Solarbio	Cat# S8010
Triethylammonium bicarbonate	Sigma	Cat# T7408
Iodoacetamide	Sigma	Cat# I1149
Formic acid	Sigma	Cat# 56302
Trifluoroacetic Acid	Sigma	Cat# 302031
Trypsin	Promega	Cat# V5280
Acetonitrile	Fisher	Cat# A998-4
TRIzol	Thermo	Cat# 15596018
Critical commercial assays		
Protein A Magnetic beads	MCE	Cat# HY-K0203
Cell Counting Kit-8 (CCK-8)	APExBIO	Cat# K1018
C_{18} Easy Tip	Micron Biotechnology Company	Cat# ETC18S096
Anti-K-la antibody conjugated agarose beads	Micron Biotechnology Company	Cat# WM102
C_{18} SPE column	Phenomenex	Cat# 8B-S123-EBJ
Deposited data		
Mass spectrometry protomics data	This paper	[PRIDE]: PXD033991
RNA-seq data	This paper	[SRA data]: PRJNA841340
Experimental models: cell lines		
AGS cells	Cell Bank of Type Culture Collection of Chinese Academy of Sciences	TCHu232
HGC-27 cells	Cell Bank of Type Culture Collection of Chinese Academy of Sciences	TCHu22

(*Continued on next page*)

Continued

REAGENT or RESOURCE	SOURCE	IDENTIFIER
MGC-803 cells	iCell Bioscience	iCell-h141
GES-1 cells	iCell Bioscience	iCell-h062
Software and algorithms		
GraphPad Prism 8	GraphPad Software	v.8.0.2
rMATS	Xing Lab	v.4.1.0
MaxQuant	www.maxquant.org/	v.1.5.2.8
InterProScan	www.ebi.ac.uk/interpro/	v.5.14-53.0
KAAS	www.genome.jp/kaas-bin/kaas_main	v.2.0
KEGG Mapper	www.kegg.jp/kegg/mapper.html	v.2.5
Wolfpsort	www.genscript.com/psort/wolf_psort.html	v.0.2
Netsurfp	https://services.healthtech.dtu.dk/service.php?NetSurfP-1.0	v.1.0
Perl module	https://metacpan.org/pod/Text::NSP::Measures::2D::Fisher	v.1.31

RESOURCE AVAILABILITY

Lead contact

Further information and requests for resources and reagents should be directed to and will be fulfilled by the lead contact, Yongbin Ding (njdyb@njmu.edu.cn).

Materials availability

This study did not generate new unique reagents.

Data and code availability

- The mass spectrometry proteomics data has been deposited to the ProteomeXchange Consortium via the PRIDE partner repository, RNAseq data has been deposited at Sequence Read Archive (SRA, NCBI). The accession numbers are listed in the Key resources table. They are available upon request if access is granted.
- This paper does not report original code.
- Any additional information required to reanalyze the data reported in this paper is available from the Lead contact upon request.

EXPERIMENTAL MODEL AND SUBJECT DETAILS

Cell lines

Gastric cancer AGS and HGC-27 cell lines were purchased from the Cell Bank of Type Culture Collection of the Chinese Academy of Sciences. Gastric epithelial GES-1 cells and gastric cancer MGC-803 cells were purchased from iCell Bioscience Inc (Shanghai, China). AGS cells were cultured in Dulbecco's modified Eagle medium (DMEM) (Gibco, Grand Island, NY). GES-1, MGC-803, and HGC-27 cells were cultured in RPMI 1640 medium (Gibco) in a humidified atmosphere containing 5% CO_2 at 37 °C. Both media were supplemented with 10% fetal bovine serum (Gibco), 100 U/mL penicillin, and 100 μg/mL streptomycin.

METHOD DETAILS

Western blot

Gastric cancer cells were treated with sodium lactate (Aladdin Biochemical Technology, Shanghai, China) or vehicle at the indicated concentrations for 24 h, then washed with phosphate-buffered saline (PBS) and lysed with radioimmunoprecipitation assay (RIPA) buffer (Thermo Fisher Scientific, Waltham, MA, USA). Samples (10 μg each) were separated with SDS-PAGE electrophoresis. The membranes were blocked with 3% skim milk at room temperature for 1 h, then incubated overnight at 4°C with primary

antibodies: anti-Kla (Micron Biotechnology Company, Hangzhou, China), anti-hnRNPA1 (ABclonal, Wuhan, China), anti-SF3B1 (ABclonal), and anti-β-Actin (ABclonal). Membranes were then incubated with HRP Goat Anti-Rabbit IgG secondary antibody (ABclonal) for 1 h at room temperature. The blot was developed with ECL substrate (Yeasen, Shanghai, China) and photographed with a Molecular Imager (Bio-RAD, Hercules, CA, USA) or X-ray film exposure.

RNA-seq

AGS cells were treated with sodium lactate (20 mM) or vehicle for 24 h, then washed with PBS and collected. There were three biological replicates for each group. Total RNA was extracted using TRIzol Reagent (Thermo Fisher Scientific) following the manufacturer's instructions. Transcriptome sequencing was conducted on an Illumina platform by GENEWIZ (Suzhou, China). rMATS (http://rnaseq-mats.sourceforge.net/) was used to analyze the RNA-seq data and identify differential alternate splicing events, including skipped exon (SE), alternative 5′ splice site (A5SS), alternative 3′ splice site (A3SS), mutually exclusive exon (MXE), and retained intron (RI) events. rMATS was used to calculate the p value and false discovery rate (FDR) for differences in the isoform ratio of each gene. Events with $|IncLevelDifference| \geq 0.02$, p value ≤ 0.001, and FDR ≤ 0.05 were classified as differential alternative splicing events.

Immunoprecipitation (IP)

Protein A magnetic beads (MedChem Express, Shanghai, China) were pre-incubated for 2 h at room temperature with primary antibodies: IgG control (AB), anti-hnRNPA1 (ABclonal), or anti-SF3B1 (ABclonal). AGS cells were pretreated with sodium lactate or vehicle for 24 h, then washed with PBS and lysed with cell lysis buffer to perform western blot and IP (Beyotime, Shanghai, China). Samples were sonicated and centrifuged at 13,000 x g for 15 min at 4°C. The supernatants were collected to obtain the protein samples. These samples were then incubated with the magnetic beads and rotated at 4°C overnight. The magnetic beads were washed with PBS + Tween (PBST) five times before adding 5× SDS loading buffer and boiling the samples for 10 min. The prepared samples were then used for western blot.

Immunohistochemistry (IHC) staining

Pre-prepared tissue microarrays were deparaffinized and hydrated, then washed with PBS. Microwave antigen retrieval was performed in citric acid buffer. Endogenous peroxidase was then blocked with 3% H_2O_2 for 30 min, and microarrays were incubated with 5% serum containing 0.5% bovine serum albumin (BSA). Microarrays were incubated with primary antibodies at 4°C overnight. After washing with PBS three times, microarrays were incubated with secondary antibody for 1 h at room temperature. Finally, microarrays were stained with 3, 3′-diaminobenzidine (DAB) and counterstained with hematoxylin.

An IHC kit was obtained from ORIGENE (Beijing, China). The microarrays were photographed with an Axio Scope A1 (Zeiss, Germany). The intensities of IHC staining were determined with Image Pro plus v6.0, then divided by the whole area of the tissue slice in each image to calculate relative Kla levels. Tissue arrays were provided by the Nanjing Pukou Central Hospital and approved by the Ethics Committee of the Nanjing Pukou Central Hospital.

Sample preparation for LC-MS/MS

Three independent cultured replicates of AGS cells were harvested and mixed. The cells were sonicated with lysis buffer (a cocktail of 8 M urea, 50 mM Tris 8.0, 1% NP40, 1% NaDOC, 10 mM EDTA, and 1% protease inhibitor). Lysates were centrifuged at 20,000 x g at 4°C for 10 min, and the supernatant was collected as the raw protein sample. Dithiothreitol (DTT) was added to a final concentration of 10 mM to the protein samples, which were then incubated at 37°C for 60 min. Samples were cooled to room temperature before adding 30 mM Iodoacetamide (IAM), then incubated at room temperature in the dark for 45 min. Proteins were precipitated with 5× volume cold acetone, then washed with 80% cold acetone three times. The supernatants were discarded and extracted proteins were incubated at room temperature for 10 min.

Peptide fractionation and affinity enrichment

Proteins were dissolved in 0.1 M triethylammonium bicarbonate (TEAB) solution and sonicated on ice. Trypsin was then added at a ratio of 1:50 trypsin:protein (w/w) and samples were incubated at 37°C overnight. Trifluoroacetic Acid (TFA) was then added to a final concentration of 1% to terminate the reaction. Samples were desalted with a C_{18}SPE column and eluted peptides were dried with a vacuum concentrator.

Peptides were then redissolved and enriched with anti-L-lactyllysine antibody-conjugated agarose beads (Micron Biotechnology Company). Finally, the bonded lactated peptides were eluted, dried with a vacuum concentrator, redissolved, desalted with a C18 EasyTip, and dried with a vacuum concentrator.

LC-MS/MS analysis

Peptides were dissolved in 100% H_2O plus 0.1% Formic acid (FA) then centrifuged at 20,000 x g. Supernatants were tested with LC-MS on the Ultimate RSLC nano 3000 coupled with the Thermo Scientific Q Exactive HFX (Thermo Fisher Scientific). Enriched peptides were separated using the Thermo Acclaim PepMap RSLC C18 column (75 um × 500 mm, 2 μm, Thermo Fisher Scientific) at 40°C. The mobile phase was composed of 100% H_2O plus 0.1% FA (A) and 80% acetonitrile (ACN) plus 0.1% FA (B). The gradient program was set as follows: 0–6 min, 2–10% solution B; 6–51 min, 10–20% solution B; 51–58 min, 20–80% solution B; 58–62 min, 80% solution B; 62–63 min, 80–2% solution B; 63–70 min, 2% solution B. The flow rate was 250 μL/min.

The Orbitrap was applied to detect whole peptides and ion fragments at resolutions of 60,000 and 30,000, respectively. The electrospray voltage was set to 2.0 kV. Automatic gain control (AGC) was used to prevent overfilling of the iontrap. The m/z range was from 350–1800 for MS scans. The MS fixed first mass was set at 110 m/z. The affinity enrichment and LC-MS/MS analyses were conducted by the Micron Biotechnology Company.

Database searching

The raw MS/MS data were analyzed with MaxQuant (v.1.5.2.8) (http://www.maxquant.org/). The tandem mass spectra were collected and compared against the *Homo sapiens* database from UniProt. Mass errors of fragment ions and precursors were set to 0.02 Da and 5 ppm. Trypsin/P was specified as the cleavage enzyme with the following limitations: four missing cleavages, five modifications per peptide, and five charges. Carbamidomethylation was set as a fixed modification for cysteine and lactylation on lysine was set as a variable modification. The minimal peptide length was set as seven. The FDR thresholds for modification sites, peptides, and proteins were set at 1%. Kla sites with localization probability < 0.75 and MaxQuant scores < 40 were excluded.

Bioinformatics analysis

WoLF PSORT was used to predict the subcellular localization of each protein. Using GO annotations (www.ebi.ac.uk/GOA/), proteins were classified using three categories: biological processes, cellular components, and molecular functions. The KEGG database was used to identify biochemical pathways of proteins with Kla. Netsurfp-1.0 was used to analyze the secondary structures and surface accessibilities of peptides. Enrichment in biological pathways and functional annotations were tested with a two-tailed Fisher's exact test; categories with a corrected p value < 0.05 were considered statistically significant.

QUANTIFICATION AND STATISTICAL ANALYSIS

Sample numbers used for statistical analysis are depicted in the figures. GraphPad Prism 8 was used to make statistical comparisons with Student's t test, one-or two-way ANOVA and Fisher's exact test (depicted in figure legends). Data are presented as the means +/− SD. Significance values are *p < 0.05, **p < 0.01 and ***p < 0.001.